Parameter Optimization for the Induction Magnetometer of 10 kHz to 100 kHz

WENBIN LI[1], PU HUANG[2], ZHONGYI DING[1], AND YUEDONG XIE[2], (Member, IEEE)
[1]Laboratory of Low Frequency Electromagnetic Communication Technology with the WMCRI, CSSC, Wuhan 430079, China
[2]School of Instrumentation and Optoelectronic Engineering, Beihang University, Beijing 100191, China

Corresponding author: Pu Huang (huang_pu@buaa.edu.cn)

ABSTRACT The induction magnetometers are widely applied for magnetotelluric detection due to the characteristics of wide frequency band, large detection depth range and small size. However, the key part of the induction magnetometers – the magnetic core has eddy current loss and hysteresis loss, which significantly affects the sensitivity of the induction magnetometers. In order to improve the sensitivity of the induction magnetometers at high frequencies, this paper investigates various parameters related to the performance of the induction magnetometers working at 10 kHz to 100 kHz. Moreover, optimization method is proposed to realize the development of a wide-band, high-sensitivity, and low-noise induction magnetometer. First of all, the parameters related to the sensitivity of the sensor are investigated according to the law of electromagnetic induction. A three-dimensional finite element (3D-FE) simulation model was established to study the influence of various parameters of induction magnetometers. In addition, an analysis method combining orthogonal experiment and response surface method is adopted to reduce the quantity of computations and improve the efficiency of analysis. The orthogonal experiment is able to obtain preliminary optimal parameters with only a small amount of computation results. Based on the results of the orthogonal experiment, the response surface method is used to illustrate the relationship between the sensor parameters and losses, and hence the optimal sensor parameters can be obtained. Finally, the model is verified by other sets of simulations, and the results show the regression coefficient of the model $R^2 = 0.9735$, indicating the effectiveness of the proposed model.

INDEX TERMS Induction magnetometers, three-dimensional finite element simulation model, orthogonal experiment, response surface method, loss analysis.

I. INTRODUCTION

With the development of geophysical science and the growth of human demand for resources, deep exploration of the crust and mantle is crucial. Investigating the movement laws of continental plates, exploiting natural resources, protecting the environment, and reducing losses caused by geological disasters are the main goals of contemporary earth sciences. As an important geological exploration method, magnetotelluric detection method plays an irreplaceable role in the exploration of resources, the detection of deep geological structures, the prediction of earthquakes and the prevention and control of geological disasters [1], [2].

There are many types of magnetotelluric methods, including time domain electromagnetic method (TEM), frequency domain electromagnetic method, and direct current

The associate editor coordinating the review of this manuscript and approving it for publication was Su Yan.

method [3]–[5]. Among of these methods, frequency domain electromagnetic method is based on the theory of magnetotelluric method.

There are three main types of magnetic field receivers in frequency domain electromagnetic method based on the principle of magnetic measurement, namely fluxgate magnetometers, superconducting magnetometers including DC quantum interferometers and induction magnetometers [6]–[9].

Compared with other types of magnetic sensors, induction magnetometers have the characteristics of easy manufacture and installation, small size, light weight and low production cost. Moreover, induction magnetometers are widely applied in ground exploration due to its wide frequency band and high sensitivity.

At present, many companies produce induction magnetometers for underground detection. The frequency range of the MFS-06 induction magnetometers from Metronix in

Germany is 0. 0001 Hz to 10 kHz, and the noise level is $10pT/\sqrt{Hz}$ @ 0.01 Hz [10], [11]. Phoenix Company in Canada developed the MTC-50H induction magnetometers. Its frequency range can reach 0.0002 Hz to 40 k Hz, and the noise level is $20pT/\sqrt{Hz}$ @0.01 Hz [12]. Grosze *et al.* investigated an ultra-low power and miniaturized induction magnetometers [13]. The noise level at 1 Hz is $14pT/\sqrt{Hz}$ and that of 100 Hz to 2 kHz arrives at $350fT/\sqrt{Hz}$. Paperno *et al.* proposed a three-axis a crosstalk compensation method for induction magnetometers to improve the sensitivity [14]. In addition, magnetic feedback technology is applied to flatten the frequency response. However, negative feedback technology will increase the complexity of the magnetometer and its power consumption. Shi *et al.* investigated the induction magnetometer in the frequency band from 1 mHz to 10 kHz. Compared with the well-known sensor MFS-06, the best induction magnetometer has a smaller size and similar noise equivalent magnetic induction (NEMI) level [15]. Yan et al optimizes the winding diameter and the number of turns of the coil to achieve a sensitivity of $7pT/\sqrt{Hz}$ within a 200 Hz bandwidth, and the designed coil only has a mass of 0.44 kg [16]. Reference [17] established the equivalent input magnetic noise model (EIMN) of the 0.1 mHz to 1 Hz inductive magnetic sensor. Duan proposed an adaptive backtracking search algorithm to solve the optimization problem of an induction magnetometer [18]. Seran *et al.* designed and manufactured a satellite-borne three-axis magnetic field sensor with a weight of 430g and a working frequency range of 1 Hz ∼20 kHz [19]. Zhang *et al.* applied related algorithms to analyze the detection signals of induction magnetometers to determine whether there is unexploded ordnance underground [20]. Liu *et al.* designed an electromagnetic induction based resonant MEMS magnetometer. The overall magnetic field sensitivity is 1.306 mV/T, and the gain is 112 dB under ambient pressure. In addition, the power consumption is only 2.5 W and nonlinear error is 0.08% [21].

As introduced previously, majority of the work of induction magnetometers focused on the frequency range from an extremely low frequency to 10 kHz. To our best knowledge, there is rare work related to the frequency range from 10 kHz to 100 kHz. In fact, as the key component of the induction magnetometers, the magnetic core has a large loss at high frequencies (10 kHz-100 kHz), which greatly limits the high-frequency performance of the magnetic sensor. In order to further increase the capability of induction magnetometer at high frequencies, it is urgent to study the influence mechanism of inductive sensors on high-frequency loss. This paper analyzes the main influencing factors of the loss of induction magnetometers and determine the optimal sensor parameters based on finite element simulation. According to the law of electromagnetic induction, the influencing factors of loss include the type of material, the excitation frequency, the lift-off, and the size of the magnetic core. In order to reduce the number of simulations and improve the efficiency of analysis, an analysis method combining orthogonal experiment and response surface method is adopted. On one hand, the
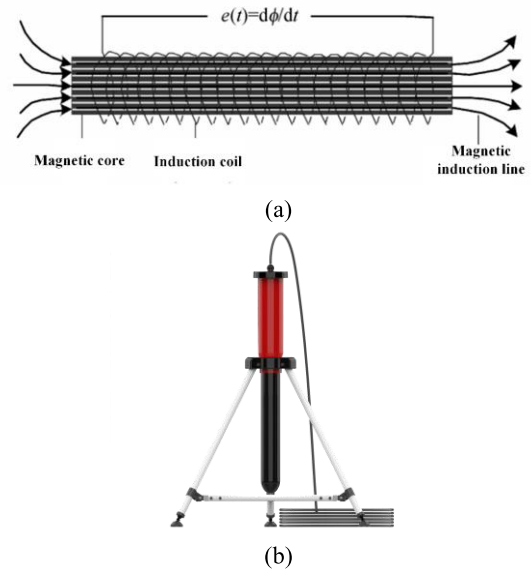

(a)

(b)

FIGURE 1. The scheme diagram of induction magnetometer (a) Sensor schematics (b) Photo of the induction magnetometer.

orthogonal test method is applied to analyze the results of representative simulation data to derive a better level combination. On the other hand, the response surface method is applied to establish the regression model for each parameter and loss at the optimal level combination based on the results of the orthogonal experiment. In addition, the model can be further used to analyze the degree of influence of various factors on loss. Finally, other sets of simulations are applied to validate the model. The regression coefficient of the model $R^2 = 0.9735$, which shows the effectiveness of the proposed model.

II. SENSOR PARAMETER ANALYSIS

As shown in Figure 1, the principle of magnetic measurement of induction magnetometers is based on Faraday's law of electromagnetic induction. When the magnetic flux of the closed loop changes, the induced current is generated in the loop. The magnetic flux always impedes the change trend of the original magnetic flux, and the induced current plays a negative feedback effect on the change of the magnetic flux of the loop. The expression of induced electromotive force is

$$e(t) = \frac{d\psi}{dt} = \frac{d(BS)}{dt} = NS_0 \frac{dB}{dt} \qquad (1)$$

where ψ is the magnetic flux of the loop. t is time. S_0 is the cross-sectional area of the core. N is the number of turns of the induction coil. When the magnetic field waveform is sine and the angular frequency is ω, the frequency domain expression of the induced voltage is

$$e(t) = i\omega NS_0 \mu_a B_0 \qquad (2)$$

where B_0 is the component of the magnetic flux density in the air in the direction of the magnetic core, and μ_a represents
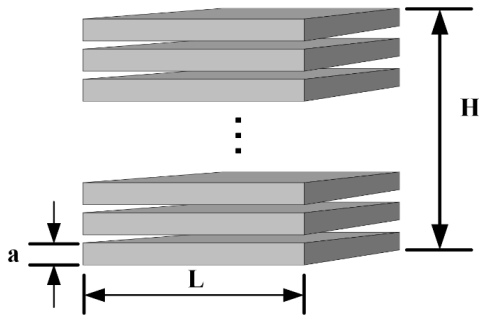
FIGURE 2. The laminate structure of the magnetic core.

the average value of the effective magnetic permeability of the magnetic core.

An important indicator for the performance of the induction magnetometers is sensitivity. The sensor output voltage corresponding to the unit magnetic induction intensity is defined as sensitivity, which can be expressed as equation (3).

$$\frac{e}{B_0} = i\omega N S_0 \mu_a \tag{3}$$

It can be seen from the above equation that the sensitivity of the magnetic core is related to the excitation frequency, the type and size of the magnetic core. In addition, different lift-off will cause changes in the magnetic flux density of the magnetic core. In fact, another important indicator of induction magnetometer is core loss, which can also reflect the sensitivity of the sensor. More specifically, induction magnetometers have a higher measurement sensitivity for low-loss magnetic cores. When the loss of the magnetic core increases, the sensitivity will decrease. The loss of magnetic materials mainly includes hysteresis loss and eddy current loss. In order to reduce the loss of the magnetic core and optimize the sensor design, it is necessary to analyze the loss.

Hysteresis loss refers to the elastic rotation of the magnetic domain in the material with the largest magnetization in the direction of the external magnetic field **H** during the magnetization process of the soft magnetic material. It is converted into magnetic potential and stored in the magnet. The magnitude of the hysteresis loss is related to the frequency of the magnetizing field, the amplitude of the magnetic field, and the magnetic material itself, which can be expressed as

$$W_h = 4/3f\eta H_m \tag{4}$$

where f is the frequency of the magnetic field, η is the Rayleigh coefficient, which is related to the core material. H_m is the magnetic field amplitude, which is affected by the lift-off.

The alternating magnetic field will induce eddy current in the core. Eddy current consumes energy on the resistance of the magnetic core, and this energy loss is called eddy current loss. In general, the magnetic core adopts a laminated structure shown as in Figure 2. Since the magnetic core is laminated and insulated between layers, eddy current loss can be reduced to a certain extent. As for the laminate
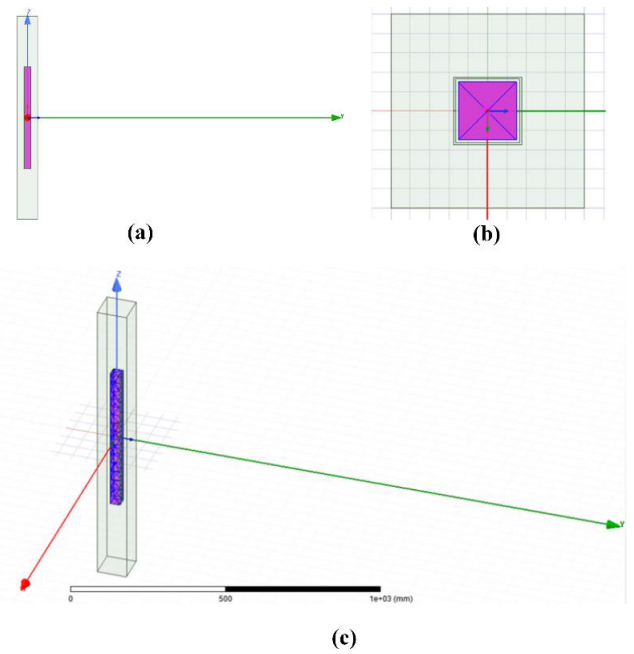

FIGURE 3. Three-dimensional finite element model for induction magnetometer. (a) Main view (b) Top view (c) Stereograph.

core structure, the eddy current loss can be calculated by equation (5).

$$P_{e2} = \frac{n\pi^2 a^2}{8\rho} f^2 B_m^2 \tag{5}$$

In the equation, a is the thickness of the laminate and ρ is the resistivity. Based on the above analysis, it can be found that the loss of the sensor is also affected by the excitation frequency, lift-off, the size and type of coil. The influence of excitation frequency on magnetic core sensor is very significant. If the excitation frequency is relatively low, the induced potential of the sensor is weak, which is not conducive to the acquisition of the signal. As for high-frequency excitation signal, it is not only exists skin effect affecting the detection sensitivity, but also serious loss. Another parameter affecting the sensor is the material of the magnetic core. Different materials have different conductivity, permeability and loss curves. In addition, the size of the sensor will also affect the sensitivity of the sensor. Different sizes will have different effective sensing areas. In fact, the core material and excitation frequency will also affect the induction area because of skin depth. Therefore, these parameters are correlated to affect the performance of the sensor. It is necessary to establish a model that can not only independently characterize the significance of parameters, but also characterize the correlation between parameters.

III. FINITE ELEMENT MODEL
A 3D-FEM model of the induction magnetometers was established by using Ansys Maxwell. The finite element method is based on the principle of variation, dividing the sensitive

TABLE 1. The properties of magnetic core material.

Material	B_s/T	$H_c/A\times\mathrm{m}^{-1}$	u_i	ρ	$T_c/°\mathrm{C}$
Mn-Zn Ferrite	0.38	9.6	3000	$1\sim10\times10^{-6}\,\Omega/\mathrm{m}$	150
Fe-based amorphous alloy	1.56	2.0	50000	$130\times10^{-6}\,\Omega/\mathrm{cm}$	410
Silicon steel sheet	1.8	<100.0	7000	$4.4\times10^{-6}\,\Omega/\mathrm{cm}$	400
Nanocrystalline iron-based alloy	1.45	0.64	10^6	$115\times10^{-6}\,\Omega/\mathrm{cm}$	570

field into a finite number of small regular units [22]–[24]. A collection of simple and regular units is used to represent the field to be solved. By analyzing each unit and establishing the unit solution equation, the solution equation of the overall problem is formed. The discrete solution of the original sensitive field can be obtained by solving the overall equation. The model of the induction magnetometers is shown in Fig. 3. The entire simulation model is composed of coils, magnetic cores and air. The outside of the sensor is set as the air region, so as to ensure that the continuity conditions of the outer boundary are met. The transient solver was adopted, and the excited current can be expressed as equation (6). The amplitude of the excitation current is set to 10A. whole model is divided into tetrahedral elements, and the number of mesh elements is 23596 in the whole model.

$$I = 10\sin(\omega t) \qquad (6)$$

According to the previous analysis, both the excitation frequency, size, and the type of magnetic core have a significant impact on the sensor. Therefore, different excitation frequencies, sizes and types of magnetic cores are set in the simulation. The core loss of different sensors is obtained by an iterative solver. The results of simulation are shown in Figure 4, which demonstrates that the sensor parameters significantly affect the core loss. Based on the solution of finite element method, an optimization method combining orthogonal experiment and response surface method is proposed to acquire the optimal sensor parameters and loss model of induction magnetometers in this paper.

IV. SENSOR PARAMETER OPTIMIZATION

A. ORTHOGONAL EXPERIMENT METHODOLOGY

Orthogonal experimental design is a method that applies orthogonal tables to arrange and analyze multi-factor experiments [25], [26]. The idea adopts part of the experimental data to represent all the experimental data. All experimental data are derived by analyzing the results of representative experimental data, and a better level combination can be found. The orthogonal optimization design method relies on a part of the optimization test of the orthogonality principle, so it has the characteristics of high efficiency. An orthogonal table is denoted by $L_n(q^m)$. L represents an orthogonal table, m represents the number of factors, q represents the factor level. Moreover, n represents the number of experiments, which is equal to the number of columns of the orthogonal
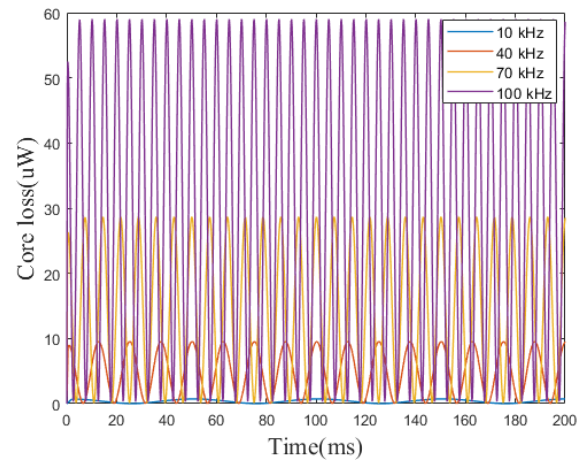

FIGURE 4. Core loss at different frequencies.

table. The type of magnetic core A (Mn-Zn Ferrite, Fe-based amorphous alloy, Nanocrystalline iron-based alloy, and Silicon steel sheet), the excitation frequency of the coil B(10 kHz, 40 kHz, 70 kHz, 100 kHz), the length of the core C(500 mm, 550 mm, 600 mm, 650 mm), the width of the core D(10 mm, 20 mm, 30 mm, 40 mm), and lift-off E(0.5 mm, 1 mm, 1.5 mm, 2 mm) are investigated. Specifically, the properties of the core material are shown in Table 1. In order to simplify and fully investigate the sensor characteristics, the orthogonal experiment with 5 factors and 4 levels, $L_{16}(5^4)$ was selected as shown in Table 2. The sum of peak value of eddy current loss and hysteresis loss (PV) was defined as the evaluation standard, and the optimal size parameter combination of the induction magnetometers was investigated.

Analysis results of the orthogonal test are listed in Table 3. The k_1, k_2, k_3, and k_4 represent the arithmetic mean values of the PV values of the four levels chosen at the same factor, respectively. Therefore, the level corresponding to the smallest k value of all factors was selected as the optimal parameter of the induction magnetometers. The optimal configuration size and excitation mode of the induction magnetometers was as follows: A: Fe-based amorphous alloy, B: 10 kHz, C: 500 mm, and D: 30 mm, and E: 1.5 mm. Among the four parameters chosen, the parameter A has the most significant effect on the PV value of the induction magnetometers. The other four parameters have similar effects on the PV value. In the subsequent analysis, Fe-based amorphous alloy is

TABLE 2. Orthogonal test table.

A	B(Hz)	C(mm)	D(mm)	E(mm)	PV (μW)
Mn–Zn Ferrite	10	500	10	0.5	11.7
Mn–Zn Ferrite	40	550	20	1.0	17.7
Mn–Zn Ferrite	70	600	30	1.5	15.1
Mn–Zn Ferrite	100	650	40	2.0	8.8
Silicon steel sheet	10	600	40	2.0	73.7
Silicon steel sheet	40	650	10	1.5	116.4
Silicon steel sheet	70	500	20	1.0	137.2
Silicon steel sheet	100	550	30	0.5	136.9
Fe-based amorphous alloy	10	500	30	1.5	1.1
Fe-based amorphous alloy	40	650	40	1.0	9.2
Fe-based amorphous alloy	70z	600	10	0.5	278.2
Fe-based amorphous alloy	100	550	20	2.0	171.1
Nanocrystalline iron-based alloy	10	600	20	2.0	1.5
Nanocrystalline iron-based alloy	40	650	30	0.5	10.8
Nanocrystalline iron-based alloy	70	500	40	1.0	23.5
Nanocrystalline iron-based alloy	100	550	10	1.5	325

FIGURE 5. The flow chart of the response surface method optimization.

selected as the core material. The relationship between other parameters and PV is determined by the response surface method based on the optimal value of the orthogonal test.

B. RESPONSE SURFACE METHODOLOGY

Response surface method is a statistical method used to deal with multivariate problem modeling based on experimental design. The response surface method can continuously analyze the various levels of the test in the process of optimizing the sensor. The nonlinear response relationship can be fitted by selecting an appropriate response surface model. The flow chart of the response surface method optimization process is shown in Figure 5.

The entire optimization process is as follows:

(I) Establish an experimental data table based on a certain experimental design method and perform the experimental design to obtain the response value.

(II)According to experimental data, create a mathematical model based on regression analysis and verify the accuracy of the model through analysis of variance

(III) The optimization algorithm is used to optimize the response value to obtain the optimal level value of each factor.

According to the analysis of the magnetic core loss and various structural parameters, it can be seen that four factors, i.e. the excitation frequency, the lift-off, the length of the magnetic core, and the width of the magnetic core, have an impact on the induction magnetometers. According to the results of the previous orthogonal test, the iron-based amorphous alloy core has the least loss, so the iron-based amorphous alloy is selected as the material of the core. The sum of eddy current loss power and hysteresis loss power will be the response value to be optimized. A response model is established between four parameters and one response value.
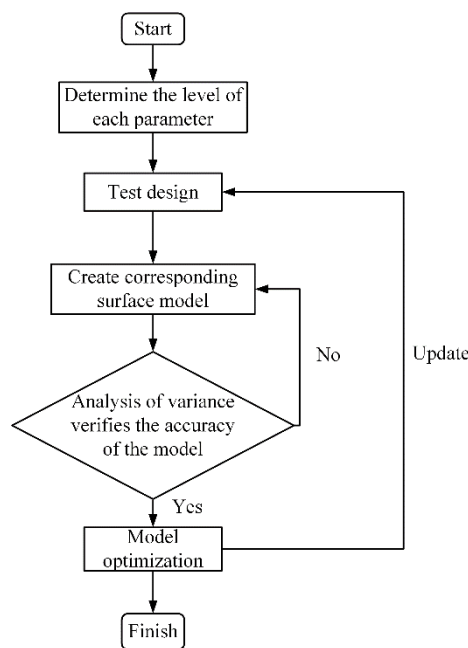
The premise of response surface optimization is to select a suitable test point. If the test points are not selected properly, it is difficult to get good optimization results. Therefore, it is particularly important to use orthogonal experiments to determine reasonable factor levels before using the response surface optimization method. According to the results of the orthogonal experiment, the reasonable value range of each factor is selected. As shown in Table 4, the lift-off is set to 1mm-2mm, the length of the magnetic core ranges from 450mm to 550mm, the width of the magnetic core ranges from 25mm to 35mm, and the excitation frequency is 10 kHz to 30 kHz.

The central composite design (CCD) is applied for the experimental design. CCD is a design method developed on the basis of 2-level full factor and partial experimental design. It can evaluate the nonlinear effects of factors and has the advantages of sequentially and high efficiency. As shown in Figure 6, the CCD test point is composed of cubic point, axial point and center point. The whole test point can be composed of the following three parts.

(I) The cube point is composed of the boundary value of each factor. There are 2^k cube points. Where k is the number of test factors.

(II) Axial points are two points on each factor coordinate axis. There are $2k$ axial points in total.

(III) The center point is to repeat the test at the center of the experimental area.

In the central combination design, each factor can take 3 levels, and the test points are widely distributed. In order to eliminate the influence of the variation range of various parameters on the experimental results, the coding transformation of each variable is carried out. Therefore, the value

TABLE 3. Analysis results of the orthogonal experiment.

Level	A(Material)	B(Frequency)	C(Core length)	D(Core width)	E(Lift-off)
k_1	13.3	22	109.4	43.4	182.8
k_2	464.2	38.5	31.0	162.8	81.9
k_3	114.9	113.5	114.4	92.1	41.0
k_4	90.2	160.5	81.5	36.3	10.8
Factors ordered by significance(R)	A(450.9) >E(172)>B(138.5)>D(119.4)>C(83.4)
Optimal solution	A: Fe-based amorphous alloy; B:10 kHz; C: 500 mm; D: 30 mm; E: 1.5 mm.

The range R is expressed as the difference between the maximum and minimum values of each factor at different levels, and the significance of each factor is determined according to the R.

TABLE 4. The coding level table of each factor.

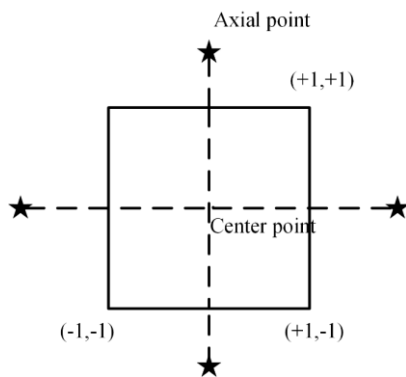| Factor		Level		
Serial number	Parameter	Low (-1)	Center (0)	High (+1)
B	Excitation frequency (kHz)	10	20	30
C	Core Length(mm)	450	500	550
D	Core width(mm)	25	30	35
E	Lift-off(mm)	1	1.5	2

FIGURE 6. Central combination test point.

range of the rectangular factor area is $(-1\ 1)$, and the level of each factor is shown in Table 4. The eddy current loss and hysteresis loss of the corresponding structural parameter induction magnetic core sensor can be directly calculated by simulating the parameters of each test points. The design and results of response surface method are shown in Table 5.

C. RESPONSE SURFACE MODEL AND ANALYSIS OF VARIANCE

In order to create the response surface model between the core loss and the structural parameters of the induction magnetometers, the order of the response surface model needs to be selected appropriately [27], [28]. Although the first-order polynomial linear response surface model has a relatively simple model structure, it can only reflect the linear relationship between input and output. In other words, it is difficult to indicate the nonlinear relationship. High-order polynomial response surface models have a better fitting accuracy, but the model is too complex, and it takes a long time to fit the response surface. Therefore, the second-order polynomial

response surface model is adopted in this work, which can not only ensure the accuracy and complete fitting of the nonlinear relationship between the structural parameters of the inductive core sensor and the core loss, but also minimize the complexity of the response surface model. The general equation of the multivariate second-order response surface model is,

$$y = \beta_0 + \sum_{i=1}^{k}\beta_i x_i + \sum_{i=1}^{k}\beta_{ii}x_i^2 + \sum_{i<j}^{k}\beta_i\beta_j x_i x_j + \varepsilon \quad (7)$$

where x and y are the factor variable and response value, respectively. k is the number of factors. The approximate error ε generally equal to zero when the engineering accuracy requirements are met.

A multivariate second-order response surface model is created as shown in equation(8). As shown in Figure 7, the correlation coefficient R^2 of regression model is 0.9636, which verifies the accuracy of the model. Table 6 is the variance of regression model. If the significance value P > 0.05, the item has no significant effect on the output in the modeling process. The main influencing factors are the excitation frequency, core length and o core width. The lift-off (0.5mm to 2mm) is an insignificant parameter to the performance of induction magnetometers at high frequencies. In order to obtain a more accurate model, the insignificant parameters in the model are eliminated. In addition, the 11th data is always larger in fitting error, and the data is ignored as well. After refitting the processed data, the response surface model equation between the sensor structure parameters and the core loss of the induction magnetometers can be expressed as equation (9). The variance analysis table of the response surface model in modified regression model is shown in Table 7. Figure 8 shows the correlation coefficient R^2 of the modified model, which is reach 0.9735. The results demonstrate the

TABLE 5. Design and results of response surface methodology.

| No.	B(kHz)	C(mm)	D(mm)	E(mm)	Loss (μW)
1	30	500	35	1.5	7.136
2	20	500	25	2.0	5.466
3	10	500	25	1.5	1.405
4	20	450	35	1.5	3.701
5	20	450	25	1.5	5.958
6	20	500	30	1.5	3.691
7	20	500	30	1.5	3.691
8	20	500	25	1.0	5.567
9	10	450	30	1.5	1.34
10	30	500	25	1.5	11.46
11	30	450	30	1.5	11.33
12	20	550	30	1.0	3.93
13	10	500	30	1.0	1.12
14	10	550	30	1.5	1.03
15	20	450	30	2.0	4.32
16	20	550	25	1.5	4.79
17	10	500	30	2.0	1.07
18	30	500	30	2.0	8.71
19	20	550	35	1.5	3.13
20	20	500	30	1.5	3.69
21	10	500	35	1.5	0.87
22	20	500	30	1.5	3.69
23	20	550	30	2.0	3.55
24	20	500	35	2.0	3.44
25	20	450	30	1.0	4.58
26	20	500	30	1.5	3.69
27	30	550	30	1.5	8.53
28	20	500	35	1.0	3.33
29	30	500	30	1.0	9.27
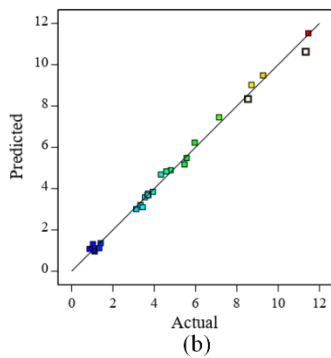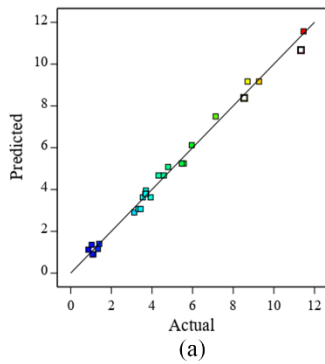
FIGURE 7. The predicted results based on the proposed core loss model. (a) Original model (b) Modified model.
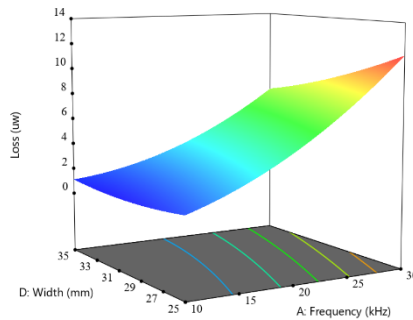
modified model is better than the initial response surface model.
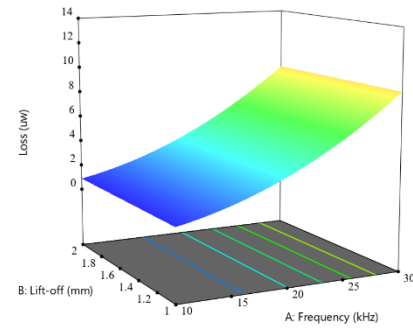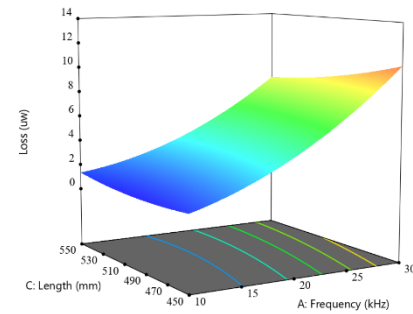
FIGURE 8. Response surface 3D image of interaction: a) lift-off and excitation frequency, b) core length and excitation frequency and c) core width and excitation frequency.

$$y = 3.69 + 4.13B - 0.1038E - 0.5223C - 1.09D$$
$$- 0.1277BE - 0.6215BC - 0.9482BD - 0.0303EC$$
$$+ 0.0527ED + 0.148CD + 1.27B^2 + 0.1553E^2$$
$$+ 0.3870C^2 + 0.3929D^2 \tag{8}$$

$$y = 3.79 + 4.13B - 0.5223C - 1.09D - 0.6215BC$$
$$- 0.9482BD + 1.24B^2 + 0.3577C^2 + 0.3635D^2 \tag{9}$$

D. PARAMETER ANALYSIS BASED ON RESPONSE SURFACE MODEL

In the response surface model, the relationship between the four parameters and the loss is analyzed. It can be seen that the most significant influence among the above factors is the

TABLE 6. Analysis of variance in regression model.

Source	Sum of squares	df	Mean square	F-value	P-value	
Model	238.88	14	17.06	157.43	<0.0001	
B	205.13	1	205.13	1892.66	<0.0001	**
C	3.27	1	3.27	30.2	<0.0001	**
D	14.19	1	14.19	130.9	<0.0001	**
E	0.1292	1	0.1292	1.19	0.2934	
BE	0.0653	1	0.0653	0.6023	0.4506	
BC	1.55	1	1.55	14.26	0.002	*
BD	3.6	1	3.6	33.19	<0.0001	**
CE	0.0037	1	0.0037	0.0338	0.8568	
DE	0.0111	1	0.111	0.1027	0.7534	
CD	0.0876	1	0.0876	0.8084	0.3838	
B2	10.48	1	10.48	96.67	<0.0001	**
C2	0.9717	1	0.9717	8.97	0.0097	*
D2	1	1	1	9.24	0.0088	*
E2	0.1564	1	0.1564	1.44	0.2495	

p-value less than 0.05 indicates that the factor is significant, which is represented by *; *p*-value less than 0.01 indicates that the factor is highly significant, which is represented by **; df: degrees of freedom, F-value: F-test value, and *p*-value: error variance.

TABLE 7. Analysis of variance in modified regression model.

Source	Sum of squares	df	Mean square	F-value	P-value	
Model	238.42	8	29.80	302.47	<0.0001	
B	205.13	1	205.13	2081.87	<0.0001	**
C	3.27	1	3.27	33.22	<0.0001	**
D	14.19	1	14.19	143.99	<0.0001	**
BC	1.55	1	1.55	15.68	0.0008	*
BD	3.6	1	3.6	36.5	<0.0001	**
B2	10.37	1	10.37	105.24	<0.0001	**
C2	0.8606	1	0.8606	8.73	0.0097	*
D2	0.8891	1	0.8891	9.02	0.0070	*

excitation frequency. In order to intuitively obtain the relationship between the excitation frequency and other factors, the response surface of the loss with the structural parameters of the sensor is shown in Fig. 8. Three groups with a greater influence were selected according to the significance of interaction term coefficients. It can be seen in Fig. 8 that the frequency of the coil had a significant interaction with three other factors. When the excitation frequency changed from 10 kHz to 30 kHz, the core length changed from 450 mm to 550 mm, the core width changed from 25 mm to 35 mm, and the lift-off changed from 1 mm to 2 mm. The loss increased with the excitation frequency. The effect of lift-off distance on loss is negligible. As the length and width of the magnetic core increase, the loss first decreases and then increases. Compared with the other factors, the frequency had a greater impact on magnetic core loss. According to the orthogonal experiment and response surface method analysis, the optimal sensor parameters can be obtained. That is, the material of core adopts Fe-based amorphous alloy. The length and width of the core is 495 mm and 31 mm, respectively. The excitation frequency is selected as 10 kHz, and the lift-off is 1.5mm. The equation (10) is applied to calculate the sensitivity of the sensor. The sensitivity of optimized sensor is $3.27 \times 10^{-3} V \cdot m/MS$.

$$S = \frac{\Delta V}{\Delta \sigma} \quad (10)$$

where ΔV represents the change of induced voltage due to the presence of metal. $\Delta \sigma$ represents the change in conductivity of the metal.

V. CONCLUSION
This study investigates an optimization method for induction magnetometers working at 10 kHz to 100 kHz based on a three-dimensional finite element simulation model. In order to improve detection sensitivity of induction magnetometers, the loss including eddy current loss and hysteresis loss is selected as the objective parameter. On one hand, the sensor is optimized by orthogonal experiment and response surface method. Orthogonal experiment is able to obtain preliminary optimal parameters through a sets of simulations. The optimal sensor parameters can be acquired through the proposed method. On the other hand, the model referred to the loss and parameters of sensor is established. It can be found that the magnetic core material and excitation frequency are the most significant parameters that affect the sensitivity of the sensor working at high frequency. Moreover, the feasibility of the proposed model is verified by other sets of simulations. The results show that the regression coefficient of the model $R^2 = 0.9735$.

REFERENCES
[1] M. Becken, O. Ritter, and H. Burkhardt, "Mode separation of magnetotelluric responses in three-dimensional environments," *Geophys. J. Int.*, vol. 172, no. 1, pp. 67–86, Jan. 2008.

[2] M. J. Nam, H. J. Kim, Y. Song, T. J. Lee, and J. H. Suh, "Three-dimensional topography corrections of magnetotelluric data," *Geophys. J. Int.*, vol. 174, no. 2, pp. 464–474, Aug. 2008.

[3] P. B. E. Sandersen, A. J. Kallesøe, I. Møller, A.-S. Høyer, F. Jørgensen, J. B. Pedersen, and A. V. Christiansen, "Utilizing the towed transient ElectroMagnetic method (tTEM) for achieving unprecedented near-surface detail in geological mapping," *Eng. Geol.*, vol. 288, Jul. 2021, Art. no. 106125.

[4] S. Yu, J. Zhang, Y. Wei, Y. Shen, and S. Wang, "A distributed phase measurement method of frequency-domain electromagnetic detection," *IEEE Trans. Instrum. Meas.*, vol. 70, Dec. 2020, Art. no. 3000711.

[5] A. Garriga, M. Linares, and J. Casanovas, "A simulation assessment of shockwave detection and damping algorithms based on magnetometers and probe vehicle data," *Transp. Res. Proc.*, vol. 52, pp. 621–628, Jan. 2021.

[6] P. Alken, N. Olsen, and C. C. Finlay, "Co-estimation of geomagnetic field and in-orbit fluxgate magnetometer calibration parameters," *Earth, Planets Space*, vol. 72, no. 1, p. 49, Dec. 2020.

[7] E. Labyt, M. Corsi, W. Fourcault, A. Laloy, F. Lenouvel, G. Cauffet, M. L. Prado, F. Berger, and S. Morales, "Magnetoencephalography with optically pumped He-4 magnetometers at ambient temperature," *IEEE Trans. Med. Imag.*, vol. 38, pp. 90–98, 2019.

[8] S. Y. Chen and T. C. Ralph, "Estimation of gravitational acceleration with quantum optical interferometers," *Phys. Rev. A, Gen. Phys.*, vol. 99, no. 2, Feb. 2019, Art. no. 023803.

[9] M. N. Kuligin, "Integrating devices in the measurement circuits of induction magnetometers," *Meas. Techn.*, vol. 61, no. 12, pp. 1209–1215, Mar. 2019.

[10] R. Wu, K. Makinwa, and J. Huijsing, "The design of a chopped current-feedback instrumentation amplifier," *Circuits Syst.*, vol. 89, pp. 1744–1755, May 2008.

[11] J. F. Witte, K. A. A. Makinwa, and J. H. Huijsing, "A CMOS chopper offset-stabilized opamp," *IEEE J. Solid-State Circuits*, vol. 42, no. 7, pp. 1529–1535, Jul. 2007.

[12] M. Dei, P. Bruschi, and M. Piotto, "Design of CMOS chopper amplifiers for thermal sensor interfacing," *Res. Microelectron. Electron.*, vol. 67, pp. 205–208, Jun. 2008.

[13] A. Grosze, E. Paperno, and S. Amrusi, "A three-axial search coil magnetometer optimized for small size, low power, and low frequencies," *IEEE Sensors J.*, vol. 11, no. 4, pp. 1088–1095, Sep. 2011.

[14] E. Paperno, A. Grosz, S. Amrusi, and B. Zadov, "Compensation of crosstalk in three-axial induction magnetometers," *IEEE Trans. Instrum. Meas.*, vol. 60, no. 10, pp. 3416–3422, Oct. 2011.

[15] H. Shi, Y. Wang, and J. Lin, "Optimal design of low-noise induction magnetometer in 1 mHz–10 kHz utilizing paralleled dual-JFET differential pre-amplifier," *IEEE Sensors J.*, vol. 16, no. 10, pp. 3580–3586, May 2016.

[16] B. Yan, W. Zhu, L. Liu, K. Liu, and G. Fang, "Design of induction magnetometer receiving sensor for through-the-earth communications," *IEEE Sensors J.*, vol. 15, no. 2, pp. 1139–1144, Feb. 2015.

[17] B. Yan, W. Zhu, L. Liu, K. Liu, and G. Fang, "Equivalent input magnetic noise analysis for the induction magnetometer of 0.1 mHz to 1 hz," *IEEE Sensors J.*, vol. 14, no. 12, pp. 4442–4449, Dec. 2014.

[18] H. Duan and Q. Luo, "Adaptive backtracking search algorithm for induction magnetometer optimization," *IEEE Trans. Magn.*, vol. 50, Dec. 2014, Art. no. 6001206.

[19] H. C. Seran and P. Fergeau, "An optimized low-frequency three-axis search coil magnetometer for space research," *Rev. Sci. Instrum.*, vol. 76, pp. 57–65, Apr. 2005.

[20] Y. Zhang, L. Collins, H. Yu, C. E. Baum, and L. Carin, "Sensing of unexploded ordnance with magnetometer and induction data: Theory and signal processing," *IEEE Trans. Geosci. Remote Sens.*, vol. 41, no. 5, pp. 1005–1015, May 2003.

[21] S. Liu, H. Liang, and B. Xiong, "An out-of-plane electromagnetic induction based resonant MEMS magnetometer," *Sens. Actuators A, Phys.*, vol. 285, pp. 248–257, Jan. 2019.

[22] R. Huang, M. Lu, A. Peyton, and W. Yin, "A novel perturbed matrix inversion based method for the acceleration of finite element analysis in crack-scanning eddy current NDT," *IEEE Access*, vol. 8, pp. 12438–12444, 2020.

[23] S. Ruoho, T. Santa-Nokki, J. Kolehmainen, and A. Arkkio, "Modeling magnet length in 2-D finite-element analysis of electric machines," *IEEE Trans. Magn.*, vol. 45, no. 8, pp. 3114–3120, Aug. 2009.

[24] J. Dong and L. D. Rienzo, "FEM and BEM implementations of a high order surface impedance boundary condition for three-dimensional eddy current problems," *IEEE Access*, vol. 8, pp. 186496–186504, 2020.

[25] Q. Wang and H. Yang, "Sensor-based recurrence analysis of energy efficiency in machining processes," *IEEE Access*, vol. 8, pp. 18326–18336, 2020.

[26] M. Khyam, S. Ge, X. Li, and M. Pickering, "Orthogonal chirp-based ultrasonic positioning," *Sensors*, vol. 17, no. 5, p. 976, Apr. 2017.

[27] K. S. Chan, S. J. Greaves, and S. Rahardja, "Techniques for addressing saddle points in the response surface methodology (RSM)," *IEEE Access*, vol. 7, pp. 85613–85621, 2019.

[28] J. T. Li, Z. J. Liu, M. A. Jabbar, and X. K. Gao, "Design optimization for cogging torque minimization using response surface methodology," *IEEE Trans. Magn.*, vol. 40, no. 2, pp. 1176–1179, Mar. 2004.

● ● ●